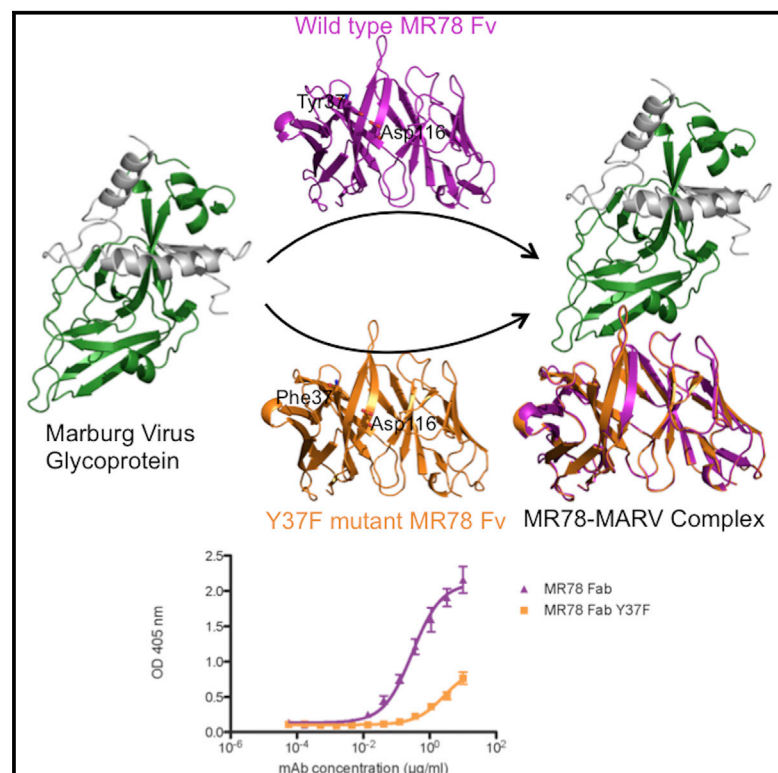


Structure

Role of Non-local Interactions between CDR Loops in Binding Affinity of MR78 Antibody to Marburg Virus Glycoprotein

Graphical Abstract



Authors

Amandeep K. Sangha, Jinhui Dong, Lauren Williamson, Takao Hashiguchi, Erica Ollmann Saphire, James E. Crowe, Jr., Jens Meiler

Correspondence

jens@meilerlab.org

In Brief

Sangha et al. have discovered that the conformation of the human antibody MR78 HCDR3 loop that binds to Marburg virus glycoprotein is stabilized by a non-local hydrogen bond between an Asp at T6 position of HCDR3 and a Tyr in HCDR1.

Highlights

- Phenix.Rosetta refinement optimizes the model of human antibody MR78
- An unusual inter-CDR loop interaction supports the bulged torso conformation of HCDR3
- Removal of inter-CDR loop H bond lowers the MR78 binding affinity by 10-fold



Role of Non-local Interactions between CDR Loops in Binding Affinity of MR78 Antibody to Marburg Virus Glycoprotein

Amandeep K. Sangha,^{1,2} Jinhui Dong,³ Lauren Williamson,⁴ Takao Hashiguchi,⁵ Erica Ollmann Saphire,^{6,7} James E. Crowe, Jr.,^{3,4,8} and Jens Meiler^{1,2,9,*}

¹Department of Chemistry, Vanderbilt University, Nashville, TN 37235, USA

²Center for Structural Biology, Vanderbilt University, Nashville, TN 37235, USA

³Vanderbilt Vaccine Center, Vanderbilt University Medical Center, Nashville, TN 37232, USA

⁴Department of Pathology, Microbiology and Immunology, Vanderbilt University Medical Center, Nashville, TN 37232, USA

⁵Department of Virology, Faculty of Medicine, Kyushu University, Fukuoka 812-8582, Japan

⁶Department of Immunology and Microbial Science, The Scripps Research Institute, La Jolla, CA 92037, USA

⁷The Skaggs Institute for Chemical Biology, The Scripps Research Institute, La Jolla, CA 92037, USA

⁸Department of Pediatrics, Vanderbilt University Medical Center, Nashville, TN 37232, USA

⁹Lead Contact

*Correspondence: jens@meilerlab.org

<https://doi.org/10.1016/j.str.2017.10.005>

SUMMARY

An atomic-detail model of the Marburg virus glycoprotein in complex with a neutralizing human monoclonal antibody designated MR78 was constructed using Phenix.Rosetta starting from a 3.6Å crystallographic density map. The Asp at T6 in the HCDR3's bulged torso cannot form the canonical salt bridge as position T2 lacks an Arg or Lys residue. It instead engages in a hydrogen bond interaction with a Tyr contributed by the HCDR1 loop. This inter-CDR loop interaction stabilizes the bulged conformation needed for binding to the viral glycoprotein: a Tyr to Phe mutant displays a binding affinity reduced by a factor of at least 10. We found that 5% of a database of 465 million human antibody sequences has the same residues at T2 and T6 positions in HCDR3 and Tyr in HCDR1 that could potentially form this Asp-Tyr interaction, and that this interaction might contribute to a non-canonical bulged torso conformation.

INTRODUCTION

Marburg virus (MARV) belongs to the Filovirus family along with a cuevavirus (Lloviu virus) and five ebolaviruses (Ebola, Sudan, Reston, Bundibugyo, and Tai Forest viruses). MARV was first discovered in 1967, and has since re-emerged multiple times to cause deadly outbreaks among humans. Recent outbreaks have been associated with up to ~90% lethality (Centers for Disease Control and Prevention (CDC), 2005), but no specific treatments are yet approved for MARV infection. Antibody therapy against filoviruses is an area of increasing interest, with many Ebola virus-specific therapies under development, including a compound currently in a clinical trial (Borio et al.,

2015). The MARV surface glycoprotein (MARV GP) consists of a trimer of glycoprotein 1 (GP1) and glycoprotein 2 (GP2) and is the only known target of protective antibodies. Recently, a number of MARV-neutralizing monoclonal antibodies from a human survivor of MARV infection were isolated and shown to bind at GP1 epitopes and to potentially inhibit the binding of the NPC1 receptor (Flyak et al., 2015). The first structure of MARV GP bound to one of these neutralizing antibodies, designated MR78, was determined using X-ray crystallography to 3.6Å resolution (Hashiguchi et al., 2015). These studies revealed the mechanism of inhibition of virus entry and paved the way for immunotherapeutic development against MARV disease.

Computational techniques (Marcatili et al., 2014; Maier and Labute, 2014; Yamashita et al., 2014; Shirai et al., 2014; Zhu et al., 2014; Sircar et al., 2009; BIOVIA, 2012; Messih et al., 2014) play an important role in constructing models for antibody/antigen complexes, as atomic detail can be lacking from experimental density maps when determined at low resolution. Antibody-modeling techniques use structure-based knowledge from high-resolution antibody structures available in the PDB to model the framework region and the six complementarity-determining regions (CDRs) of the heavy and light chains of antibody. Five out of the six CDRs typically assume canonical conformations that can be predicted from their amino acid sequence. CDR3 of the heavy chain (HCDR3), however, remains a challenge to the modeling techniques developed so far because of its variability in amino acid composition and length (Zhu et al., 2014). To overcome these limitations, rules have been proposed to classify the conformation of the base region of the HCDR3 loop, also termed the torso region (Shirai et al., 1996, 1999; Oliva et al., 1998; Morea et al., 1998; Koliashnikov et al., 2006; North et al., 2011). The torso region comprises the first three residues on the N-terminal side of HCDR3 loop after the Cys residue of framework region 3, as well as the last four residues on the C-terminal side of HCDR3 loop before the Trp residue of framework region 4 (Figure 1). According to these rules, the presence of a basic Arg/Lys residue at position T2 plus Asp at position T6 should lead to a bulged (kinked) torso,

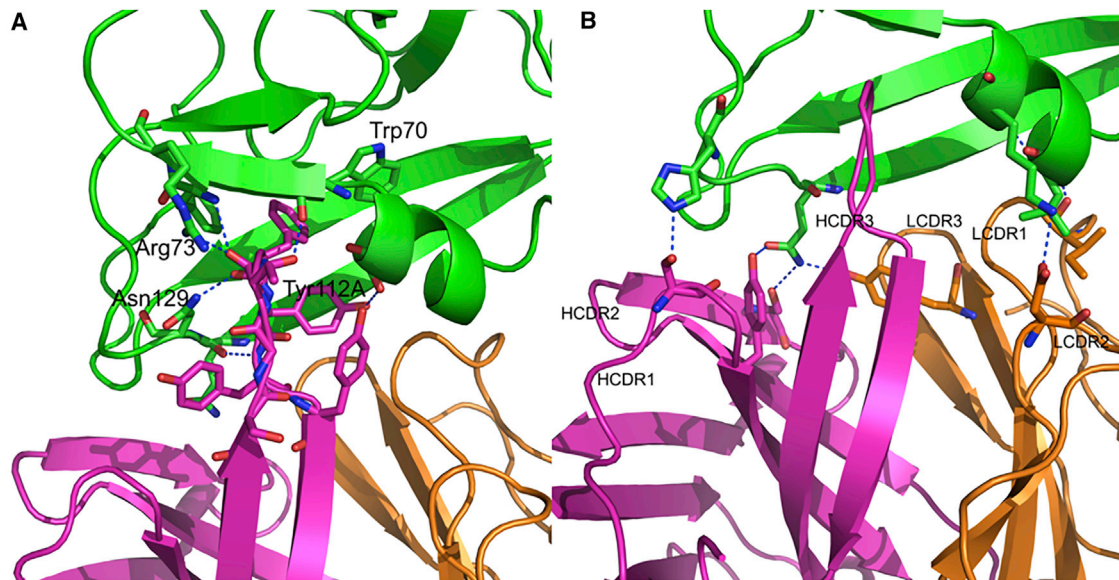


Figure 2. Antibody-Antigen Interactions in the Phenix.Rosetta Model of MARV GP1 (Green) and MR8 (Heavy Chain in Magenta and Light Chain in Orange)

(A) MR8 interacts with MARV GP1 mainly through the HCDR3 via aromatic stacking and electrostatic interactions.
 (B) The remaining five CDRs also interact with GP1 via hydrophobic and electrostatic interactions.

between MARV GP1 and MR8 occur via the HCDR3. Phe111B of MR8 HCDR3 packs between Trp70 and Phe72 of GP1 (Figure 2). Furthermore, both the experimental and the refined models indicate that additional electrostatic interactions occur between the carbonyl oxygen of MR8 Phe111B and the side chain of GP1 Asn129 and the amide nitrogen of MR8 Tyr112A with the carbonyl oxygen of GP1 Gln128. Tyr112 of HCDR3 forms a hydrogen bond with Ser67 in α helix 1 of GP1.

However, the Phenix.Rosetta model deviates from the experimental electron density map in the position of residue Arg73. In the Phenix.Rosetta model, the main-chain carbonyl oxygen of Thr111A interacts with the side chain of Arg73 of GP1. In the experimental X-ray structure, Thr111A of HCDR3 does not interact with Arg73 of GP1 (Figure 3).

Residues of the other five CDRs of MR8 also interact with GP1: Ile29 and Asn37 of LCDR1 (QASQVISNYLN) interacts with the backbone nitrogen of Leu64 and Gln126 in GP1 α helix 1, respectively, Asp56 of LCDR2 (YDTSNLKT) interacts with the side chain of Lys68 in GP1 α helix 1, Tyr107 of LCDR3 (QQYENLQFT) interacts with the side chain of GP1 Gln128 in β strand 2 and Ser35 and Tyr38 of HCDR1 (TVSGGSISSSSYYWG) interact with His131 and Gln128 of β strand 2 of GP1. Ser66 of HCDR2 (SVYSSGGAS) interacts with Gln128 of β strand 2 of GP1 (Figure 2). These additional interactions led to an increase in the predicted binding affinity of MR8 to MARV GP1 by 4 Rosetta Energy Units after Phenix.Rosetta refinement.

The six CDR conformations in the refined structure fall into canonical classes of L1-11-1, L2-8-1, L3-9-1, H1-15-1, H2-9-1, and H3-17-1, respectively. In the crystal structure, CDRs L1, L2, L3, and H3 were classified under different classes and H1 was not classifiable in the experimental structure (North et al., 2011).

Bulged Torso in MR8 HCDR3 Is Stabilized by a Hydrogen Bond between Asp116 at T6 and Tyr37 from HCDR1

One major change upon Phenix.Rosetta refinement of the experimental model of the MR8:MARV GP complex occurred in the torso region of the HCDR3 loop. The first three residues on the N-terminal side and the last four residues on the C-terminal side of HCDR3 (ASLYGSGTFYFYFYMDV) constitute the torso region. These seven residues are named T1 to T7, starting from N terminus of HCDR3 loop to the C terminus such that Ala105 is at T1 and Val117 is at T7 position (Figure 1). The refined structure shows that antibody MR8 has a bulged torso. While the torso is also bulged in the original PDB structure (PDB: 3X2D), the geometric parameters in the refined structure align much closer to the canonical values for antibody structures in Weitzner et al. (2015). Specifically, the τ_{101} is 100.3° and α_{101} is 28.2° for the refined structure. The canonical values are 101° and 39° . The values for τ_{101} and α_{101} in the four copies of MR8 in PDB: 3X2D are 124.2, 115.1, 121.7, 110.6 and -7.6 , 30.7, 11.5, -46.2 for antibody heavy chains D, H, L, and P, respectively. An unusual interaction of the Asp116 at T6 of HCDR3 with Tyr37 in the HCDR1 (TVSGGSISSSSYYWG) loop was observed. One of the four interactions, a salt bridge between Asp at T6 and Arg/Lys at T2, usually seen in bulged torso, is replaced by this inter-HCDR loop T6Asp116-Tyr37 interaction in the absence of a basic residue at T2 in MR8. The other three typical interactions observed in bulged torsos, i.e., Trp118 with carbonyl oxygen of T5 (Met115 in MR8), a backbone-backbone hydrogen bond between T2 Ser106 and T6 Asp116, and a backbone-backbone hydrogen bond between Tyr108 and Tyr114, are preserved. Thus the refined MR8 bulged torso has all of the four stabilizing hydrogen bonds present that could lead to ideal values for τ_{101} and α_{101} .

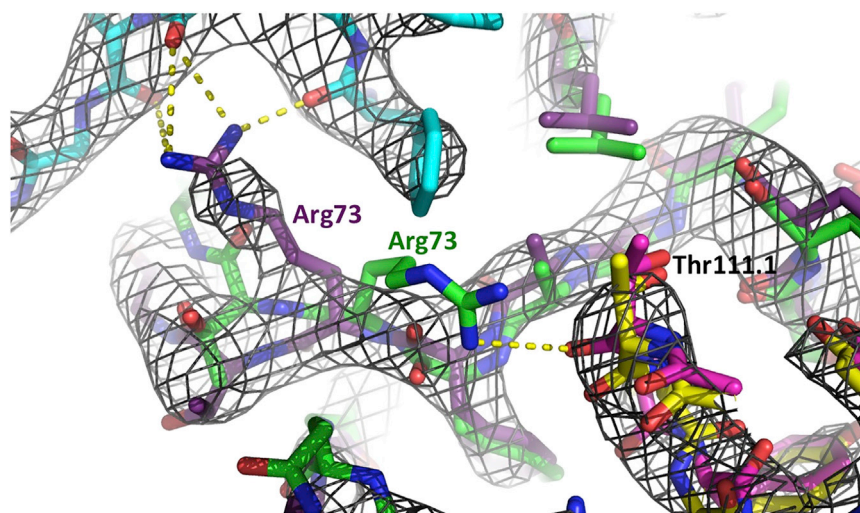


Figure 3. Superimposition of the Experimental X-ray Structure (GP1, Deep Purple; GP2, Cyan; MR78, Yellow) and the Phenix-Rosetta Refined Model (GP1, Green; MR78, Magenta) Represented by Stick Models

In black is the $2F_o - F_c$ electron density map of the MARV GP-MR78 complex, created by Phenix and illustrated using PyMOL (www.pymol.org), contoured at 1.5σ . This experimental X-ray map indicates that Arg73 (purple) interacts with GP2 (cyan), while the energy-minimized model suggests that Arg73 (green) interacts with Thr111 of HCDR3 (magenta).

A ladder of hydrogen bonds in the absence of a basic residue in the stem part between torso residues T3 and T4 can be observed in Figure 4. This HCDR3 loop structure follows the rule (iii) in Kuroda et al. (2008) and Shirai et al. (1999), which explains the effect of torso conformations on the conformation of the stem region of HCDR3 loop in antibody structure. A straight conformation of HCDR3 loop with H-bond ladder as in MR78 is infrequent in antibody structures, as the majority of the long HCDR3 loops (with >14 amino acids) adopt non-straight (bent or broad) conformations (Tsuchiya and Mizuguchi, 2016). The position of Gly111 residue is more toward the N terminus of the HCDR3 loop, as is expected for loops with a bulged torso conformation (Weitzner et al., 2015).

The HCDR1 Loop Is Stabilized in an H1-15-1 Conformation

Another region with major conformational change from the experimental structure is the HCDR1 loop. The initial Phenix.Rosetta model maintained some of the energetic frustrations for Ser34 and Ser35 residues in the HCDR1 loop stemming from the experimental coordinates (PDB: 3X2D). Therefore, the geometry of these residues in the HCDR1 loop was reconstructed using Rosetta loop modeling. The optimized HCDR1 loop residues interact with GP1 via Ser35 to His131 and Phe38 to Gln128 in β strand 2 of GP1, as mentioned above. In the original model (PDB: 3X2D), Ser35 and His131 are 4.7 Å apart. Upon remodeling, the HCDR1 loop went from not being classified under any of the clusters to H1-15-1 cluster described in North et al. (2011).

An Interaction between Phe113 in the HCDR3 Loop and Gln89 of the MR78 Light Chain Contribute to the Relative Orientation of Heavy and Light Chain in MR78

The relative orientation of heavy and light chains plays an important role in the stability of the antibody structure and its interaction with the antigen at the interface, as the HCDR3 loop stem is part of the heavy-/light-chain interface. Some interactions at the heavy- and light-chain interface are conserved among all antibody structures, e.g., the H bond between L36 Tyr and residue at T5 position (Met115 in MR78). The Phenix.Rosetta model shows an additional interaction between Gln89 of the MR78 light

chain and the carbonyl oxygen of Phe113 in the HCDR3 loop of the heavy chain (Figure 5). Hydrophobic packing between two conserved pairs of aromatic residues in the heavy and light chains is also present:

heavy chain Tyr114-Tyr55 light chain, heavy chain Trp118-Phe118 light chain. The six AB angle parameters HL, HC1, LC1, HC2, LC2, and dc for MR78, as deduced from the ABangle program (Dunbar et al., 2013), are -58.3° , 70.1° , 122.8° , 117.7° , 81.3° , and 16.8° , respectively.

Comparison of MR79 with Antibody Structures from the PDB Reveals One Other Antibody with a Similar Interaction of the Asp at T6 with Tyr from HCDR1

Interactions of torso residues with distant residues from other CDR loops may affect the torso conformation. We wanted to investigate the role of the interaction between HCDR1 Tyr and HCDR3 T6 Asp in causing or supporting the bulge in MR78. Thus, we looked for antibody structures in the PDB with similar bulged torsos as in MR78. For this purpose, we collected a set of 345 antibody structures determined at a resolution better than 3 Å, in which the T6 residue is Asp and T2 is neither Arg nor Lys. Only one antibody, termed 26-10 (PDB: 1IGJ, resolution 2.5 Å), had a bulged conformation with a similar interaction of Asp T6 with a Tyr from the HCDR1 loop (Figure 6A). Antibody 26-10 is a murine monoclonal antibody used to treat fatal digoxin (a steroid used in treatment of congestive heart failure) intoxication (Jeffrey et al., 1993). 26-10 has Asp101 at T6 and Gly94 at T2, like MR78. Although the position of these interacting Tyr residues is different in sequence between antibody 26-10 (fifth in a 13-residue-long loop) and MR78 (third last in a 15-residue-long loop), they are in close spatial proximity to Asp T6 in 3D space (Figure 6B). The τ_{101} and α_{101} values for 1IGJ are 101.1° and 49.8° , respectively. Along with T6 Asp101 to Tyr27 from HCDR1 interaction, there are only two out of three other hydrogen bonds supporting a bulged torso present in antibody 26-10: (1) a hydrogen bond between the T5 Met100B carbonyl oxygen and the Trp103 side chain and (2) a backbone-backbone hydrogen bond between T2 Gly94 and T6 Asp101. The backbone-backbone hydrogen bond between T4 Ala100A and Ser96 on the N terminus of HCDR3 loop is missing. The degree of kink ($\tau_{101} = 101.1^\circ$) with Asp-Tyr interaction present in antibody 26-10 is similar to that in refined MR78 structure and is close to the median value for τ_{101} bond-angle distributions in known antibody structures with bulged torso. The other copy

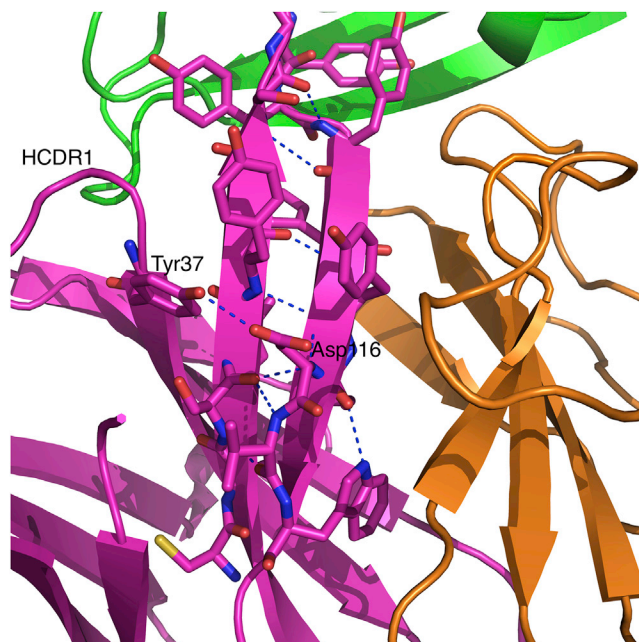


Figure 4. An Unusual Interaction of Asp116 at T6 with Tyr37 from HCDR1 Loop in the MR78 Torso Region Optimizes the Bulge

The majority of the antibody structures with bulged torso have T6 Asp interacting with local HCDR3 residues, especially with Arg/Lys at T2 if present. A non-local interaction such as T6Asp116-Tyr37 between HCDR3 and HCDR1 loops seen in MR78 is extremely uncommon in known antibody structures.

of anti-digoxin antibody in 1IGJ (chain D), however, does not show the Asp-Tyr interaction between the two HCDR loops, and the degree of kink in this chain deviates from the median value of 101° – 97.8° along with $\alpha_{101} = 50.2^\circ$.

In the PDB, we identified 27 unique heavy chains with Tyr at fifth position of a 13-amino-acid-long HCDR1 and Asp at T6 without Arg/Lys at T2 in the HCDR3 loop, as in anti-digoxin antibody. None of these antibodies make the Asp-Tyr interaction seen in MR78 or antibody 26-10 (PDB: 1IGJ, chain B). Three out of 27 have an extended torso (1UWE_H, 3C0_C, and 4FQJ_L). Of the remaining 24 antibody structures, 11 maintain at least three out of the four hydrogen-bond interactions that support the bulge and have τ_{101} closer to 101° , the median value for degree of kink in known antibody structures. In four of these 24 antibody structures, the Asp-Tyr interaction seen in 1IGJ is replaced by Asp-Arg (511L_B and 5L6Y_H) or Asp-Thr (5CEY_X and 5FYJ_H) residue immediately next to the T3 residue on the N-terminal side, and the τ_{101} value is 100.1° (5L6Y_H), 101.7° (511L_B), 102° (5FYJ_H), and 100.8° (5CEY_X), respectively.

Phenix.Rosetta Model of MR78 Agrees with Subsequently Determined High-Resolution Structure of the Apo MR78 Fab

A structure of the unbound MR78 Fab was determined at 1.9 Å resolution to test the conformation of the HCDR3 torso region and the HCDR1 in the apo state (Table 2). This unbound, apo MR78 structure also shows a bulged torso with T6Asp116-Tyr37 interaction maintained and a conformation of the HCDR1 loop similar to that of the Phenix.Rosetta model (Figure 7). The

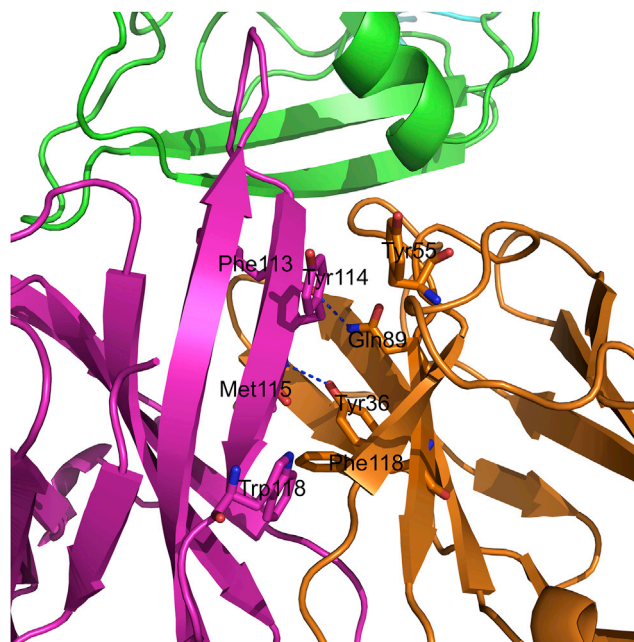


Figure 5. The Heavy (Magenta) and Light Chain (Orange) Interface Packing in MR78

Along with all the interactions conserved in antibody structures, MR78 makes an additional interaction between Gln89 of light chain and Phe113 of heavy chain.

interaction between Ser35 of HCDR1 and Tyr57 of HCDR2 seen in the experimentally determined complex was not observed in the unbound MR78 structure or the optimized model. Overall the C_α -root-mean-square deviation between the Fv region of the unbound structure and the Phenix.Rosetta bound model of MR78 was 0.73 Å.

Many antibodies use a pre-formed apo structure with minimal changes upon antigen binding to minimize the entropic cost of binding (Sela-Culang et al., 2012). Only a few antibodies are known to undergo major conformational changes, including a transformation from a non-bulged to bulged torso (BV04-01: 1cbv and 1nbv) (Herron et al., 1991). For MR78, the apex of the HCDR3 loop undergoes backbone conformational change upon binding with some side-chain reorientations for residues Thr111A, Phe111B, and Tyr112B (Figures 7B and 7C). The CG-CB-CA-N dihedral angle for the three residues differs by 100° or more between the apo and bound forms of MR78.

An MR78 Tyr37Phe Mutant Antibody Displays Slightly Increased B Factors in the HCDR Regions while Maintaining the MR78 Wild-Type Apo Conformation

To understand the effect of the non-canonical inter-HCDR T6Asp116-Tyr37 interaction seen in MR78, we determined the apo structure of MR78 Tyr37Phe mutant at 2.0 Å (Table 2). While this structure maintains the bulge in the absence of Asp-Tyr interaction, the normalized B factors in the HCDR3 loop show a small increase of 0.87 in the apex residues and 0.66 in the torso residues. From the unbound wild-type to the unbound mutant MR78 structure, the τ_{101} and α_{101} values change from 107.3° and 38.1° to 113.3° and 21.1° , respectively. As a result, the

Table 2. Unbound MR78 Wild-Type and Tyr37Phe Mutant Data Collection and Refinement Statistics

	MR78 Wild-Type	MR78 Tyr37Phe Mutant
Wavelength (Å)	0.97872	0.97856
Space group	P3 ₁ 21	P3 ₁ 21
Unit cell dimensions	a = b = 117.57, c = 91.80, α = β = 90°, γ = 120°	a = b = 117.18, c = 92.10, α = β = 90°, γ = 120°
Resolution (Å)	50.91–2.00	50.00–2.00
Highest-resolution shell (Å)	2.11–2.00	2.11–2.00
R _{sym} ^a (%)	11.2 (43.9)	7.7 (74.2)
Mean I/σ(I)	13.6 (4.9)	9.8 (1.7)
Total no. of reflections	557,044 (79,594)	278,149 (50,000)
Completeness (%)	100	99.2
Refinement Statistics		
R _{work} /R _{free} ^b (%)	17.1/19.4	18.6/21.5
Average B factor (Å ²)	33.7	52.3
Total no. of atoms	3,815	3,505
Water molecules	544	211
Bond angles (°)	0.846	0.890
Bond length (Å)	0.0034	0.0076
Ramachandran: favored/ allowed (%)	98.77/100	97.147/100

Numbers in parentheses are for the highest-resolution shell.

^aR_{sym} = $\sum \sum |I_{hkl} - \langle I_{hkl} \rangle| / \sum I_{hkl}$, where $I_{hkl(i)}$ is the observed intensity and $\langle I_{hkl} \rangle$ is the final average intensity.

^bR_{work} = $\sum ||F_{obs}| - |F_{calc}|| / \sum |F_{obs}|$ and R_{free} = $\sum ||F_{obs}| - |F_{calc}|| / \sum |F_{obs}|$, where R_{free} and R_{work} are calculated using a randomly selected test set of 5% of the data and all reflections excluding the 5% test set, respectively.

degree of kink in the loop and the position of the kink relative to the framework of the antibody are altered. In the absence of this inter-HCDR interaction in mutant MR78, the other three

hydrogen bonds supporting the bulge in the torso region are maintained, i.e., Trp118 side chain to T5 Met115 carbonyl oxygen, a backbone-backbone H bond between T4 Tyr114 and Tyr108, and a backbone-backbone H bond between T2 Ser106 and T6 Asp116. Changes in the degree of the kink in the loop, however, affect the pseudo-bond angles and torsional angles between C α atoms of the stem residues in the HCDR3 loop in the mutant MR78, i.e., HCDR3 is in a slightly different conformation and slightly more flexible in the MR78 Tyr37Phe mutant.

T6Asp116-Tyr37 Inter-CDR Loop Interaction Affects Binding Affinity of MR78

We hypothesize that the role of the Asp-Tyr interaction, in the absence of Arg/Lys at T2, is to stabilize the bulge in the conformation necessary for interaction with MARV GP, thereby reducing the entropic cost of binding. To test this hypothesis, we determined the binding affinity of the MR78 Tyr37Phe mutant and compared it with MR78 using ELISA. The shift in the concentration-response curves shows that wild-type MR78 binds to the MARV GP approximately 10-fold tighter than the MR78 Tyr37Phe mutant, supporting our hypothesis (Figure 8).

DISCUSSION

The Phenix.Rosetta optimization method provides an invaluable aid to crystallographic structure determination tools when low-resolution data challenges model building. Although it can add atomic detail not present in the experimental data with high confidence, there is also the possibility of occasional prediction of positions and contacts that are not in agreement with the electron density maps. However, this does not exclude the possibility that some of these contacts occur, perhaps transiently, in the biological environment.

The conformation of short antibody CDRs, typically HCDR1 and 2 and LCDR1, 2, and 3, can often be predicted from their sequence alone. HCDR3 is an exception as it is often between 12 and 20 residues long, sometimes longer. HCDR3s adopt kinked/bulged or extended structures. The bulge observed in the MR78 HCDR3 torso cannot be classified by the rules by

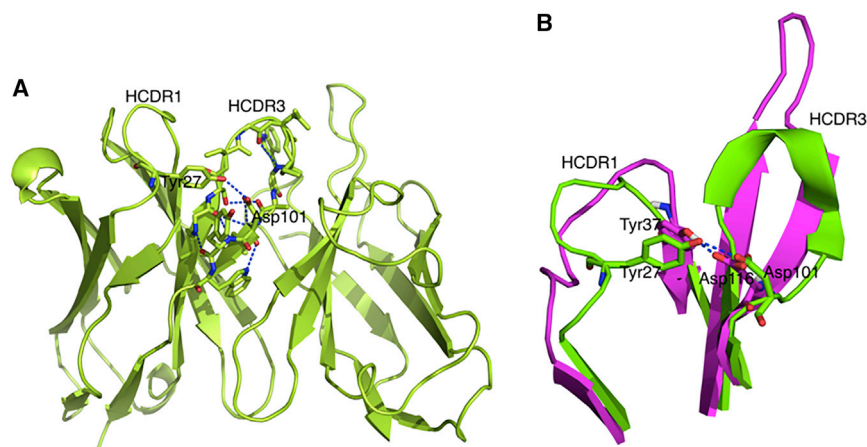


Figure 6. Comparison of HCDR3 Torso in Antibody 26-10 and MR78

(A) In the absence of a basic residue at T2, the bulge in the torso region of HCDR3 loop in antibody 26-10 (1IGJ_B.pdb) shows an interaction of Asp101 at T6 with Tyr27 from HCDR1, similar to the case of MR78.

(B) Position of the Tyr residue interacting with Asp in HCDR3 torso is different in HCDR1 sequence in MR78 (magenta) and 1IGJ (green).

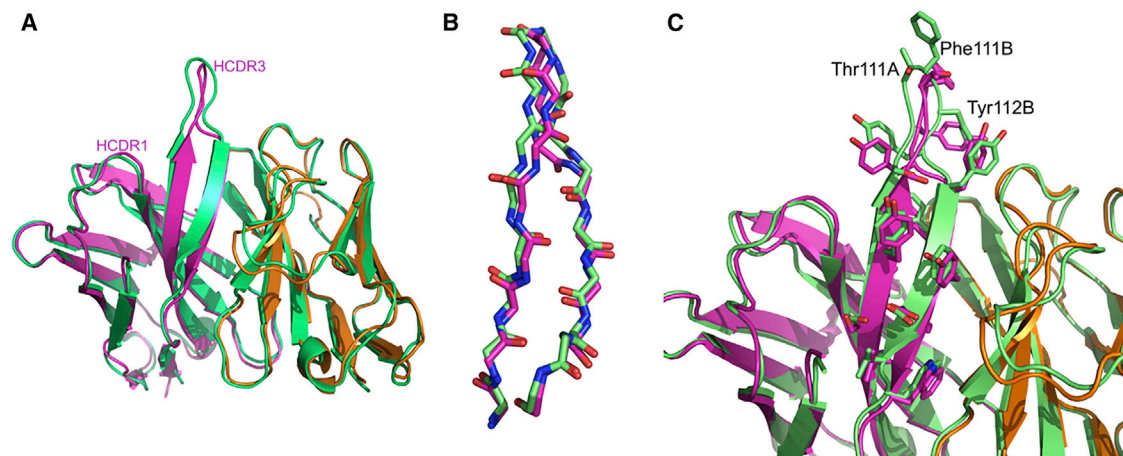


Figure 7. Structure of Apo MR78

(A) Comparison of MR78 as observed in the Phenix.Rosetta-optimized GP complex (magenta and orange) and the high-resolution apo (unbound) structure (green).

(B and C) The backbone conformation (B) and residue side-chain orientation (C) differ at the apex of HCDR3 loop in apo MR78.

Shirai et al. (1999), Kuroda et al. (2008), or North et al. (2011), as shown recently that these rules no longer hold for a large number of antibody structures. Exceptions to the H3-rule 1b have been discussed due to the interaction of Asp at T6 with other basic residues either in the HCDR3 loop itself or from light chain (positions 46 and 49) (Kuroda et al., 2008). Interactions of torso residues with distant residues seem to play a role in optimizing the bulge for better binding, as shown here in the case of MR78 antibody. Such interactions already exist in antibody 26-10 (PDB: 1IGJ) and can be expected in new antibody structures based on our analysis of the antibody sequence database. Therefore, inter-CDR loop interactions should be taken into account while classifying and modeling torso regions in the HCDR3 loop of antibody structures.

The H3-rules website (<http://www.protein.osaka-u.ac.jp/rcsfp/pi/H3-rules/>) (Shirai et al., 1999; Kuroda et al., 2008) predicts an extended torso for MR78 based on a predicted interaction between T6 Asp and Trp118, the first residue after the C terminus of HCDR3. A class A hairpin was predicted for HCDR3 without a meaningful feature such as an H-bond ladder. These results show that classification software fails to recognize the bulge in the HCDR3 torso. Effects of the surrounding environment on the torso conformation such as in the 26-10 and MR78 antibody structures can be used to improve predictions in antibody-modeling software.

A database containing 465 million human antibody sequences was analyzed to find the number of sequences with similar residues in HCDR3 torso, i.e., absence of Arg/Lys at T2 and presence of Asp at T6 position, which could potentially lead to an interaction with Tyr in the HCDR1 loop. A total of 56.5 million antibody sequences were found to have Asp (D) at T6 and not Arg/Lys at T2. Of these 56.5 million sequences, 23.7 million (5% of all human antibodies) have Tyr at third to last position in the HCDR1 loop, as in MR78, and 11.8 million sequences (2.5% of all human sequences) have Tyr at the fifth position in the HCDR1 loop, as in the 12-10 antibody. This analysis shows that this interaction between HCDR3 and HCDR1 might

contribute to the torso conformation in the structure of many human antibodies.

Conclusions

Here we present the crystal structures of the unbound MR78 Fab fragment and a point mutant of this antibody, as well as a Phenix.Rosetta refined model of the MR78-GP1 complex. The HCDR3 of MR78, as well as the previously determined 26-10 antibody, forms a bulged torso structure with an unusual interaction of Asp at the T6 position of HCDR3 with a Tyr residue in the HCDR1. Five percent of all human antibodies share sequence features consistent with this bulge conformation. The non-local interactions from HCDR1 can complement for the absence of Arg/Lys at T2 and support the bulge for better binding of the antibody.

The HCDR3 loop in MR78 is not flexible due to its H-bond ladder structure and does not undergo large backbone conformational changes upon binding to MARV GP. The tip, however, adjusts to maximize the aromatic stacking interactions.

Energy minimization in Phenix.Rosetta allows improvement of model geometry in the moderate-resolution X-ray structure, especially in the HCDR3 torso. Energy minimization, however, predicts a few additional contacts between MR78 and GP1 that are contradicted by electron density maps and do not appear in any of the four independent copies of the MR78-GP1 complex in the asymmetric unit. Formation of these contacts would improve the energetics of binding. It is striking, then, that the experimental electron density maps do not support all the possible contacts that could be made. The crystals were grown at pH 6.5, which itself likely would not significantly affect binding. It may be that the biological complex is not energetically “ideal.” Alternatively, the additional contacts between HCDR1 and GP1 may be transient and not captured in the crystal structure. Nonetheless, all the structures and models indicate that the HCDR3 possesses an atypical bulge containing particular contacts of the HCDR3 to HCDR1. This non-local interaction defines the structural determinants of the interaction of the HCDR3 loop

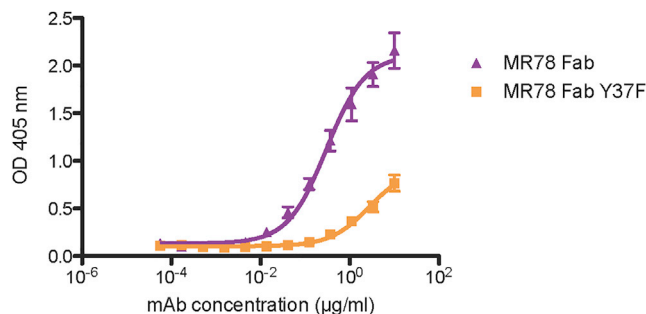


Figure 8. Binding of MR78 Fab and MR78 Tyr37Phe Fab to MARV GP
MR78 Fab binds MARV GP with an EC_{50} value of 0.30 $\mu\text{g}/\text{mL}$ (95% confidence interval: 0.22–0.42 $\mu\text{g}/\text{mL}$) and MR78 Tyr37Phe Fab binds MARV GP with an EC_{50} value of 2.71 $\mu\text{g}/\text{mL}$ (95% confidence interval: 1.77–4.15 $\mu\text{g}/\text{mL}$), resulting in a 10-fold reduction in binding to MARV GP. EC_{50} values of MR78 and MR78 Tyr37Phe Fab to MARV GP were obtained via ELISA. Technical triplicates of each were performed. Plates were coated with 1 $\mu\text{g}/\text{mL}$ MARV GP. MR78 and MR78 Tyr37Phe Fab molecules were serially diluted 3-fold from 10 $\mu\text{g}/\text{mL}$ to 56.5 ng/mL. EC_{50} values and 95% confidence intervals were calculated using a non-linear regression analysis of the curves generated in Prism v.5 (GraphPad Software). Graphpad Prism software was used to determine average values, standard errors, and standard deviations.

with the antigen and is therefore key for antibody efficacy. These models provide a starting point for computational design of antibodies against MARV disease. Antibody-modeling software can include new rules to take into account the long distant interactions of torso residues, resulting in better antibody models.

STAR★METHODS

Detailed methods are provided in the online version of this paper and include the following:

- KEY RESOURCES TABLE
- CONTACT FOR REAGENT AND RESOURCE SHARING
- EXPERIMENTAL MODEL AND SUBJECT DETAILS
 - Cells
- METHOD DETAILS
 - Phenix.Rosetta Refinement of 3X2D
 - HCDR1 Loop Modeling
 - MR78 Fab Production and Purification
 - Crystallization, Data Collection, and Structure Determination
 - Half-maximal Effective Concentration (EC_{50}) Binding ELISA Analysis
- QUANTIFICATION AND STATISTICAL ANALYSIS
- DATA AND SOFTWARE AVAILABILITY

SUPPLEMENTAL INFORMATION

Supplemental Information includes Supplemental Methods and can be found with this article online at <https://doi.org/10.1016/j.str.2017.10.005>.

AUTHOR CONTRIBUTIONS

A.K.S. and J.M. planned research. A.K.S., J.D., and L.W. performed research. A.K.S., J.D., L.W., and J.M. analyzed the data. A.K.S., J.D., L.W., T.H., E.O.S., J.E.C., and J. M. wrote the paper.

ACKNOWLEDGMENTS

A.K.S. is grateful to Dr. Frank DiMaio for technical discussions on the Phenix.Rosetta refinement technique, and to Jessica Ann Finn, Alexander Sevy, and Alberto Cisneros for helpful discussions. The work was supported through NIH grants R21 AI121799 (J.M.), U19 AI117905 (J.E.C. and J.M.), U19 AI109711 (J.E.C.), and DTRA grant HDTRA1-13-1-0034 (J.E.C.). Work in the Sapphire laboratory is supported through NIH U19AI1097652 and R01 AI089498. This research used resources of the Advanced Photon Source, a US Department of Energy (DOE) Office of Science User Facility operated for the DOE Office of Science by Argonne National Laboratory under contract number DE-AC02-06CH11357. Updated coordinates for the MR78-MARV GP complex, including additional insights from separate work (L.B. King et al., unpublished data), have been deposited in the PDB under PDB: 5UQY.

Received: January 6, 2017

Revised: August 17, 2017

Accepted: October 23, 2017

Published: November 16, 2017

REFERENCES

- Adams, P.D., Afonine, P.V., Bunkoczi, G., Chen, V.B., Davis, I.W., Echols, N., Headd, J.J., Hung, L.W., Kapral, G.J., Grosse-Kunstleve, R.W., et al. (2010). PHENIX: a comprehensive Python-based system for macromolecular structure solution. *Acta Crystallogr. D Biol. Crystallogr.* 66, 213–221.
- Bender, B.J., Cisneros, A., Duran, A.M., Finn, J.A., Fu, D., Lokits, A.D., Mueller, B.K., Sangha, A.K., Sauer, M.F., Sevy, A.M., et al. (2016). Protocols for molecular modeling with Rosetta3 and RosettaScripts. *Biochem* 55, 4748–4763.
- BIOVIA. (2012). Discovery Studio Modeling Environment, 3.5 ed (Accelrys Software).
- Borio, L., Cox, E., and Lurie, N. (2015). Combating emerging threats - accelerating the availability of medical therapies. *N. Engl. J. Med.* 373, 993–995.
- Centers for Disease Control and Prevention (CDC). (2005). Outbreak of Marburg virus hemorrhagic fever—Angola, October 1, 2004–March 29, 2005. *MMWR* 54, 308–309.
- Chen, V.B., Arendall, W.B., 3rd, Headd, J.J., Keedy, D.A., Immormino, R.M., Kapral, G.J., Murray, L.W., Richardson, J.S., and Richardson, D.C. (2010). MolProbity: all-atom structure validation for macromolecular crystallography. *Acta Crystallogr. D Biol. Crystallogr.* 66 (Pt 1), 12–21.
- DiMaio, F., Echols, N., Headd, J.J., Terwilliger, T.C., Adams, P.D., and Baker, D. (2013). Improved low-resolution crystallographic refinement with Phenix and Rosetta. *Nat. Methods* 10, 1102–1104.
- DiMaio, F., Song, Y., Li, X., Brunner, M.J., Xu, C., Conticello, V., Egelman, E., Marlovits, T.C., Cheng, Y., and Baker, D. (2015). Atomic-accuracy models from 4.5-Å cryo-electron microscopy data with density-guided iterative local refinement. *Nat. Methods* 12, 361–365.
- Dunbar, J., Fuchs, A., Shi, J., and Deane, C.M. (2013). ABangle: characterising the VH-VL orientation in antibodies. *Protein Eng. Des. Sel.* 26, 611–620.
- Emsley, P., and Cowtan, K. (2004). Coot: model-building tools for molecular graphics. *Acta Crystallogr. D Biol. Crystallogr.* 60, 2126–2132.
- Flyak, A.I., Ilinykh, P.A., Murin, C.D., Garron, T., Shen, X.L., Fusco, M.L., Hashiguchi, T., Bornholdt, Z.A., Slaughter, J.C., Sapparapu, G., et al. (2015). Mechanism of human antibody-mediated neutralization of Marburg virus. *Cell* 160, 893–903.
- Hashiguchi, T., Fusco, M.L., Bornholdt, Z.A., Lee, J.E., Flyak, A.I., Matsuoka, R., Kohda, D., Yanagi, Y., Hammel, M., Crowe, J.E., and Sapphire, E.O. (2015). Structural basis for Marburg virus neutralization by a cross-reactive human antibody. *Cell* 160, 904–912.
- Herron, J.N., He, X.M., Ballard, D.W., Blier, P.R., Pace, P.E., Bothwell, A.L., Voss, E.W., Jr., and Edmundson, A.B. (1991). An autoantibody to single-stranded DNA: comparison of the three-dimensional structures of the unliganded Fab and a Deoxynucleotide-Fab complex. *Proteins* 11, 159–175.
- Jeffrey, P.D., Strong, R.K., Sieker, L.C., Chang, C.Y.Y., Campbell, R.L., Petsko, G.A., Haber, E., Margolies, M.N., and Sheriff, S. (1993). 26-10 Fab-

- Digoxin complex - affinity and specificity due to surface complementarity. *Proc. Natl. Acad. Sci. USA* **90**, 10310–10314.
- Kaufmann, K.W., Lemmon, G.H., DeLuca, S.L., Sheehan, J.H., and Meiler, J. (2010). Practically Useful: what the ROSETTA protein modeling suite can do for you. *Biochem* **49**, 2987–2998.
- Koliasnikov, O.V., Kiral, M.O., Grigorenko, V.G., and Egorov, A.M. (2006). Antibody CDR H3 modeling rules: extension for the case of absence of Arg H94 and Asp H101. *J. Bioinform. Comput. Biol.* **4**, 415–424.
- Kuroda, D., Shirai, H., Kobori, M., and Nakamura, H. (2008). Structural classification of CDR-H3 revisited: a lesson in antibody modeling. *Proteins* **73**, 608–620.
- Maier, J.K., and Labute, P. (2014). Assessment of fully automated antibody homology modeling protocols in molecular operating environment. *Proteins* **82**, 1599–1610.
- Marcatili, P., Olimpieri, P.P., Chaillyan, A., and Tramontano, A. (2014). Antibody structural modeling with prediction of immunoglobulin structure (PIGS). *Nat. Protoc.* **9**, 2771–2783.
- McCoy, A.J., Grosse-Kunstleve, R.W., Adams, P.D., Winn, M.D., Storoni, L.C., and Read, R.J. (2007). Phaser crystallographic software. *J. Appl. Crystallogr.* **40**, 658–674.
- Messih, M.A., Lepore, R., Marcatili, P., and Tramontano, A. (2014). Improving the accuracy of the structure prediction of the third hypervariable loop of the heavy chains of antibodies. *Bioinformatics* **30**, 2733–2740.
- Morea, V., Tramontano, A., Rustici, M., Chothia, C., and Lesk, A.M. (1998). Conformations of the third hypervariable region in the VH domain of immunoglobulins. *J. Mol. Biol.* **275**, 269–294.
- North, B., Lehmann, A., and Dunbrack, R.L. (2011). A new clustering of antibody CDR loop conformations. *J. Mol. Biol.* **406**, 228–256.
- Oliva, B., Bates, P.A., Querol, E., Aviles, F.X., and Sternberg, M.J.E. (1998). Automated classification of antibody complementarity determining region 3 of the heavy chain (H3) loops into canonical forms and its application to protein structure prediction. *J. Mol. Biol.* **279**, 1193–1210.
- Sela-Culang, I., Alon, S., and Ofra, Y. (2012). A systematic comparison of free and bound antibodies reveals binding-related conformational changes. *J. Immunol.* **189**, 4890–4899.
- Shirai, H., Ikeda, K., Yamashita, K., Tsuchiya, Y., Sarmiento, J., Liang, S.D., Morokata, T., Mizuguchi, K., Higo, J., Standley, D.M., and Nakamura, H. (2014). High-resolution modeling of antibody structures by a combination of bioinformatics, expert knowledge, and molecular simulations. *Proteins* **82**, 1624–1635.
- Shirai, H., Kidera, A., and Nakamura, H. (1996). Structural classification of CDR-H3 in antibodies. *FEBS Lett.* **399**, 1–8.
- Shirai, H., Kidera, A., and Nakamura, N. (1999). H3-rules: identification of CDR-H3 structures in antibodies. *FEBS Lett.* **455**, 188–197.
- Sircar, A., Kim, E.T., and Gray, J.J. (2009). RosettaAntibody: antibody variable region homology modeling server. *Nucleic Acids Res.* **37** (Web Server issue), W474–W479.
- Tsuchiya, Y., and Mizuguchi, K. (2016). The diversity of H3 loops determines the antigen-binding tendencies of antibody CDR loops. *Protein Sci.* **25**, 815–825.
- Wang, R.Y., Kudryashev, M., Li, X., Egelman, E.H., Basler, M., Cheng, Y., Baker, D., and DiMaio, F. (2015). De novo protein structure determination from near-atomic-resolution cryo-EM maps. *Nat. Methods* **12**, 335–338.
- Weitzner, B.D., Dunbrack, R.L., and Gray, J.J. (2015). The origin of CDR H3 structural diversity. *Structure* **23**, 302–311.
- Winn, M.D., Ballard, C.C., Cowtan, K.D., Dodson, E.J., Emsley, P., Evans, P.R., Keegan, R.M., Krissinel, E.B., Leslie, A.G.W., McCoy, A., et al. (2011). Overview of the CCP4 suite and current developments. *Acta Crystallogr. D Biol. Crystallogr.* **67**, 235–242.
- Yamashita, K., Ikeda, K., Amada, K., Liang, S.D., Tsuchiya, Y., Nakamura, H., Shirai, H., and Standley, D.M. (2014). Kotai Antibody Builder: automated high-resolution structural modeling of antibodies. *Bioinformatics* **30**, 3279–3280.
- Zhu, K., Day, T., Warshaviak, D., Murrett, C., Friesner, R., and Pearlman, D. (2014). Antibody structure determination using a combination of homology modeling, energy-based refinement, and loop prediction. *Proteins* **82**, 1646–1655.

STAR★METHODS

KEY RESOURCES TABLE

REAGENT or RESOURCE	SOURCE	IDENTIFIER
Antibodies		
MR78 wild-type	Flyak et al., 2015	NA
MR78 mutant	This paper	NA
Goat anti-human kappa-alkaline phosphatase	Southern Biotech	2060-04
Chemicals, Peptides, and Recombinant Proteins		
Papain	Thermo Fisher Scientific	CAT #44985
Hitrap Protein G HP column 1ml	GE Healthcare	Cat # 29-0485081
CaptureSelect CH1 column 1ml	Thermo Fisher Scientific	Cat# 494346201
Full-length extracellular domain MARV GP	Flyak et al., 2015	NA
Deposited Data		
Crystal structure of MR78 wildtype	This paper	PDB ID: 5JRP
Crystal structure of MR78 mutant	This paper	PDB ID: 5WEQ
Experimental Models: Cell Lines		
Human hybridoma MR78 wild type	Flyak et al., 2015	NA
Expi293F Cells	Thermo Fisher Scientific	Cat# A14527
Recombinant DNA		
MR78 mutant	Genscript	NA
Software and Algorithms		
Phenix.Rosetta_refine	DiMaio et al., 2013	https://www.rosettacommons.org
Phaser	McCoy et al., 2007	https://www.phenix-online.org/documentation/reference/phaser.html
Phenix	Adams et al., 2010	https://www.phenix-online.org/documentation/reference/refinement.html
Coot	Emsley and Cowtan, 2004	https://www2.mrc-lmb.cam.ac.uk/personal/pemsley/coot/
Molprobrity	Chen et al., 2010	http://molprobrity.biochem.duke.edu/

CONTACT FOR REAGENT AND RESOURCE SHARING

Further information and requests for resources and reagents should be directed to and will be fulfilled by the Lead Contact, Jens Meiler (jens@meilerlab.org).

EXPERIMENTAL MODEL AND SUBJECT DETAILS

Cells

The human hybridoma cell line expressing MR78 mAb was grown in post-fusion medium ((ClonaCell-HY Medium E, STEMCELL Technologies #03805), and was then expanded in serum free medium (Hybridoma-SFM, GIBCO #12045-076) at 37°C with 7% CO₂. MR78 mutant Fab was produced with Expi293F cells (Thermo Fisher Scientific #A14527) grown in Epi293 Expression Medium (ThermoFisher Scientific #A1435104) at 37°C with 7% CO₂.

METHOD DETAILS

Phenix.Rosetta Refinement of 3X2D

Phenix software is used to determine protein structures from X-ray scattering data, although modeling some regions using moderate- to low-resolution scattering data still remains a challenge. The combined Phenix.Rosetta refinement approach

(DiMaio *et al.*, 2013) has been shown to improve model geometry (with better Rfree factor and Molprobit score) for structures determined in the resolution range of 3.0 – 4.5 Å. For the 3.6 Å structure of MARV GP in complex with antibody MR78 (PDB ID 3X2D), we used the *low_resolution_refinement* script (available at [Rosetta/source/src/apps/public/crystal_refinement/](https://www.rosettacommons.org/docs/latest/rosetta_apps_public/crystal_refinement/)) with symmetry. A weight of 20 was used for the *elec_dens_fast* option to reweight scoring function with electron density data. The XML script and options used for refinement are explained in DiMaio *et al.* (*Nature Methods*, 2013). The resulting model then was dual-space relaxed to generate 100 additional models. The lowest energy model was chosen as the optimized model for the MR78:MARV GP complex.

HCDR1 Loop Modeling

The HCDR1 loop residues still showed energetic frustrations after Phenix.Rosetta refinement and dual-space relaxation. The loop modeling technique (Kaufmann *et al.*, 2010) in Rosetta was used to rebuild the 10 residue-long HCDR1. A thousand models were generated that grouped into five clusters. A representative structure from the largest cluster (size 263) was chosen as the final model. The HCDR1 then was grafted onto the MR78:MARV GP structure and the complex was relaxed to generate 100 additional models. The lowest scoring model was chosen as the final model to analyze antibody-antigen interactions.

MR78 Fab Production and Purification

The human hybridoma cell line expressing MR78 mAb was grown in post-fusion medium, as previously described (Flyak *et al.*, 2015). HiTrap MabSelectSure columns were used to purify MR78 from filtered hybridoma supernates. The purified MR78 mAb was cleaved with papain to obtain the MR78 Fab fragment (Pierce Fab Preparation Kit, ThermoFisher Scientific), and the MR78 Fab was purified further with IgG-CH1 affinity chromatography (CaptureSelect, ThermoFisher Scientific).

Crystallization, Data Collection, and Structure Determination

MR78 Fab and MR78 mutant (12 mg/mL in 20 mM Tris, 7.5, 50 mM NaCl) was crystallized in 4.1 ~ 4.5 M NaCl, 0.1 M HEPES, pH 7.5 with protein to precipitant volume ratio of 1.5:1. Crystals were flash frozen in liquid nitrogen using Parabar 10312 oil as cryoprotectant. Diffraction data were collected at the beamline 21-ID-F at the Advanced Photon Source. The diffraction data were processed with imosflm, XDS and CCP4 suite (Winn *et al.*, 2011). The crystal structure was solved by molecular replacement using the MR78 structure in the MR78 and the MARV GP complex (PDB ID 3X2D) with the program Phaser (McCoy *et al.*, 2007). The structure was refined and rebuilt manually with Phenix (Adams *et al.*, 2010) and Coot (Emsley and Cowtan, 2004), respectively. The final statistics of final structures of wild type and mutant MR78 Fabs are shown in Table 2. The models have been deposited into the Protein Data Bank (PDB ID 5JRP and 5WEQ).

Half-maximal Effective Concentration (EC₅₀) Binding ELISA Analysis

The soluble form of the full-length extracellular domain of MARV GP (1 µg/µL) was diluted in 1x D-PBS to coat 384-well ELISA plates (Thermo Scientific #265202) at 25 µL/well and incubated at 4°C overnight. The plates were washed 3x with D-PBS-T (1x DPBS + 0.05% Tween 20) and blocked for 1 hour at room temperature with blocking solution (1% non-fat dry milk (Blotting Grade Blocker Bio-rad #170-6404), 1% goat serum (Gibco 16210-072) in D-PBS-T). After blocking, the plates were then washed 3x with D-PBS-T and 25 µL/well of 3-fold serially diluted purified Fab MR78 or Fab MR78 Tyr37Phe (10 µg/mL – 56.5 ng/mL) in blocking solution was added. Plates were incubated for 2 hours at room temperature and then washed 3x with D-PBS-T. Secondary antibody (goat anti-human kappa-alkaline phosphatase conjugated; Southern Biotech 2060-04) at a 1:4,000 dilution in blocking solution was added at 25 µL/well for 1 hour at room temperature. Alkaline phosphatase substrate solution (phosphatase substrate tablets (Sigma #S0942) in AP substrate buffer (1M Tris aminomethane (Fisher #BP152-5), 0.3 mM MgCl₂ (Sigma #M1028)) was added at 25 µL/well following plate washing 4x with D-PBS-T. Plates were incubated at room temperature in the dark for 2 hours then read at an optical density of 405 nm with a Biotek plate reader. EC₅₀ values and 95% confidence intervals were calculated using a non-linear regression analysis of the curves generated in Prism v.5. (GraphPad Software).

QUANTIFICATION AND STATISTICAL ANALYSIS

Graphpad Prism software was used to determine average values, standard errors, and standard deviations for Figure 8.

DATA AND SOFTWARE AVAILABILITY

The structure factors and experimental model have been deposited in the RCSB Protein Data Bank under PDB: 5JRP, PDB: 5WEQ and PDB: 5UQY. Rosetta software is available at <https://www.rosettacommons.org>. Updated coordinates for the MR78-MARV GP complex, including additional insights from separate work (L.B. King *et al.*, unpublished data), have been deposited in the PDB under PDB: 5UQY.